

Article

# Catalytic Behaviour of Ce-Doped Ni Systems Supported on Stabilized Zirconia under Dry Reforming Conditions

Ahmed Sadeq Al-Fatesh <sup>1,\*</sup>, Yasir Arafat <sup>1,\*</sup>, Ahmed Aidid Ibrahim <sup>1</sup>,  
Samsudeen Olajide Kasim <sup>1</sup>, Abdulrahman Alharthi <sup>2</sup>, Anis Hamza Fakieha <sup>1</sup>,  
Ahmed Elhag Abasaeed <sup>1</sup>, Giuseppe Bonura <sup>3</sup> and Francesco Frusteri <sup>3</sup>

<sup>1</sup> Chemical Engineering Department, College of Engineering, King Saud University, P.O. Box 11421 Riyadh, Saudi Arabia; aidid@ksu.edu.sa (A.A.I.); sofkolajide2@gmail.com (S.O.K.); anishf@ksu.edu.sa (A.H.F.); abasaeed@ksu.edu.sa (A.E.A.)

<sup>2</sup> College Sciences and Humanities, Prince Sattam Bin Abdulaziz University, Al-Kharj 11942, Saudi Arabia; a.alharthi@psau.edu.sa

<sup>3</sup> CNR-ITAE, Istituto di Tecnologie Avanzate per l'Energia "Nicola Giordano", Via S. Lucia sopra Contesse 5, 98126 Messina, Italy; giuseppe.bonura@ita.cnr.it (G.B.); francesco.frusteri@ita.cnr.it (F.F.)

\* Correspondence: aalfatesh@ksu.edu.sa (A.S.A.-F.); engryasir@ksu.edu.sa (Y.A.); Tel.: +966114676859 (A.S.A.-F. & Y.A.); Fax: +966114678770 (A.S.A.-F. & Y.A.)

Received: 19 April 2019; Accepted: 16 May 2019; Published: 22 May 2019



**Abstract:** Ni supported on bare and modified  $ZrO_2$  samples were synthesized using the incipient wet impregnation method. The  $t\text{-}ZrO_2$  phase was stabilized by incorporation of  $La_2O_3$  into  $ZrO_2$ . Moreover, the influence of  $CeO_2$ -doping on the physico-chemical and catalytic properties under  $CO_2$  reforming conditions was probed. The characterization data of the investigated catalysts were obtained by using XRD,  $CO_2/H_2$ -TPD, BET, TPR, TPO, TGA, XPS and TEM characterization techniques. In the pristine Ni/Zr catalyst, the  $t\text{-}ZrO_2$  phase transformed into the monoclinic phase. However, upon support modification by  $La_2O_3$ , significant effects on the physicochemical properties were observed due to the monoclinic-to-tetragonal  $ZrO_2$  phase transformation also affecting the catalytic activity. As a result, superior activity on the  $La_2O_3$  modified Ni/Zr catalyst was achieved, while no relevant change in the surface properties and activity of the catalysts was detected after doping by  $CeO_2$ . The peculiar behavior of the Ni/ $La\text{-}ZrO_2$  sample was related to higher dispersion of the active phase, with a more pronounced stabilization of the  $t\text{-}ZrO_2$  phase.

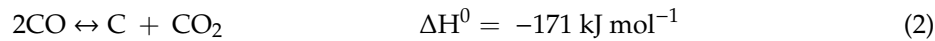
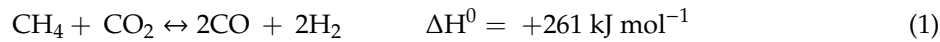
**Keywords:**  $CO_2$  reforming; Ni-catalyst; syngas; tetragonal zirconia; phase stabilization

## 1. Introduction

Modern civilization is confronted with two major challenges: dwindling energy resources [1,2] and global warming caused by greenhouse gases (mainly  $CH_4$  and  $CO_2$ ) [3,4]. The dry reforming of the methane (DRM) reaction for the conversion of greenhouse gases into a valuable synthesis gas ( $H_2$  and  $CO$ ) product is a potential contestant for confronting both these challenges simultaneously. Syngas is recognized as the building block for the production of  $H_2$  and liquid fuels such as olefins, paraffins, methanol, oxygenates and aromatics in the petrochemical industry, employing the Fischer–Tropsch synthesis process [5,6].

It is an acknowledged fact that DRM is hampered by some side reactions, such as the Boudouard reaction (Equation (2)), water gas shift reaction (Equation (3)), and methane decomposition

(Equation (4)), which are considered the major reactions leading to the deactivation of catalysts as a result of coke deposition [7].



Coke formation represents a serious problem in DRM. Therefore, noble metal catalysts like Ir, Pt, Rh, Ru and Pd, based on anti-coking properties, were used to constrain such phenomena [8]. In spite of their marvelous characteristics, noble metals are rare and expensive, and end up with a higher cost-benefit ratio. Therefore, the application of noble metals is no longer commercially feasible. On the other hand, Ni-based catalysts are cheap and abundant, and also demonstrate an interesting catalytic performance for the DRM reaction. Unfortunately, nickel particles undergo thermal sintering and tend to promote coke formation over the catalyst surface, leading to catalyst deactivation. Therefore, besides the relevance of active metal components, the role of support material is crucial in inhibiting (or at least limiting) the formation of coke. This can be accomplished by: modifying the electronic properties of the catalyst through a control of the metal-support interaction [9]; improving the oxygen storage capacity [10]; or controlling the size of active metal particles [11]. Consequently, several oxide supports, like  $\text{Al}_2\text{O}_3$ ,  $\text{SiO}_2$ ,  $\text{ZrO}_2$ ,  $\text{CeO}_2$  and  $\text{La}_2\text{O}_3$  have been employed to enhance the catalytic activity and stability of Ni catalysts. Among different oxides,  $\text{ZrO}_2$  is extensively employed as a functional support, possessing several unique properties like redox properties, acid-base bi-functional properties, thermal and mechanical stability, high ionic conductivity and oxygen transport properties, making it a favourable support for reforming reactions [12,13]. Moreover, the partial  $\text{CO}_2$  activation, as well as the strong anchoring effects endowed by  $\text{Zr}^{4+}$ , may effectively boost the DRM reaction. However, it was found that Ni/ $\text{ZrO}_2$  catalysts undergo serious coke formation over their surface, leading to fast deactivation and, subsequently, reactor plugging [14,15].

The deactivation of the catalyst may occur for several reasons, for instance, commonly available  $\text{ZrO}_2$  possesses a rather smaller surface area (viz.  $<50 \text{ m}^2/\text{g}$ ) in comparison to its counterparts [16,17]. Moreover,  $\text{ZrO}_2$  is characterized by three polymorph structures, named as the monoclinic phase ( $m\text{-ZrO}_2$ , room temperature–1175 °C), tetragonal phase ( $t\text{-ZrO}_2$ , 1175–2370 °C), and cubic phase ( $c\text{-ZrO}_2$ , 2370–2680 °C) [18]. The  $c\text{-ZrO}_2$  is poorly stable at room temperature, which restricts its large scale application in catalysis as compared to  $m\text{-ZrO}_2$  and  $t\text{-ZrO}_2$ . Furthermore,  $t\text{-ZrO}_2$  is found to have a better performance than  $m\text{-ZrO}_2$  [19]. In addition,  $t\text{-ZrO}_2$  is widely utilized as a support for Ni catalysts in  $\text{CH}_4$  reforming processes, even if its thermodynamic instability represents a problem to overcome. Rezaei et al. proposed that the surface energy difference between monoclinic and tetragonal phases may induce the  $t\text{-ZrO}_2$  phase to be thermodynamically stable for tiny crystals [20]. Consequently, in order to exploit the excellent properties associated with  $\text{ZrO}_2$  support, it is essential to find a way to prepare high surface area  $\text{ZrO}_2$  and stabilizing  $t\text{-ZrO}_2$ , which will obviously contribute to enhancing the catalytic performance.

Recently, heteroatom oxide compounds (e.g.,  $\text{Y}_2\text{O}_3$ ,  $\text{CeO}_2$ ,  $\text{TiO}_2$  and  $\text{K}_2\text{O}$ ) have been reported to stabilize  $t\text{-ZrO}_2$  in catalytic processes [19,21]. When  $\text{La}_2\text{O}_3$  is assigned to modify the support for the dry reforming reaction, the ability of support to activate  $\text{CO}_2$  was enhanced by means of  $\text{La}_2\text{O}_2\text{CO}_3$  formation. In this way, it discards the accumulated carbon through oxidation of coke at the Ni- $\text{La}_2\text{O}_3$  interface [22,23].

Furthermore, in order to promote the oxygen storage capacity of  $\text{ZrO}_2$ , as well as to enhance the thermal stability of Ni-based catalysts,  $\text{CeO}_2$  was proposed as a promoter (in fact, ceria demonstrates outstanding redox properties as a result of a quick transition between  $\text{Ce}^{4+}/\text{Ce}^{3+}$ ).

The purpose of this study was to exploit the aforementioned peculiar properties of  $\text{ZrO}_2$  support, trying to circumvent the limitations associated with its instability and low surface area. To achieve this objective, high surface area  $\text{ZrO}_2$  supported Ni catalysts were prepared using the incipient wet-impregnation method. Subsequently,  $\text{ZrO}_2$  support was modified by heteroatom oxides, like  $\text{La}_2\text{O}_3$ , with an intention that it might stabilize the  $t\text{-ZrO}_2$  phase. In addition, 1%  $\text{CeO}_2$  promoter was also incorporated to enhance the oxygen storage capacity of catalysts. Consequently, the unique properties achieved as an outcome of the synergistic effect of the ceria promoter and high surface area  $\text{ZrO}_2$  support modifiers ( $\text{La}_2\text{O}_3$ ) were studied to stabilize  $t\text{-ZrO}_2$  and their eventual influence on the catalytic performance.

## 2. Results and Discussion

### 2.1. Physicochemical Features of the Ceria Promoted $\text{Ni}/x\text{-Zr}$ ( $x = 0, \text{La}_2\text{O}_3$ ) Catalysts

Figure 1a illustrates the X-ray diffraction patterns of fresh catalyst samples. The diffraction peaks of  $\text{NiO}$  can be featured on the diffractograms at  $2\theta = 37.3^\circ$  and  $43.3^\circ$  corresponding to the [101] and [012] reflections, respectively.

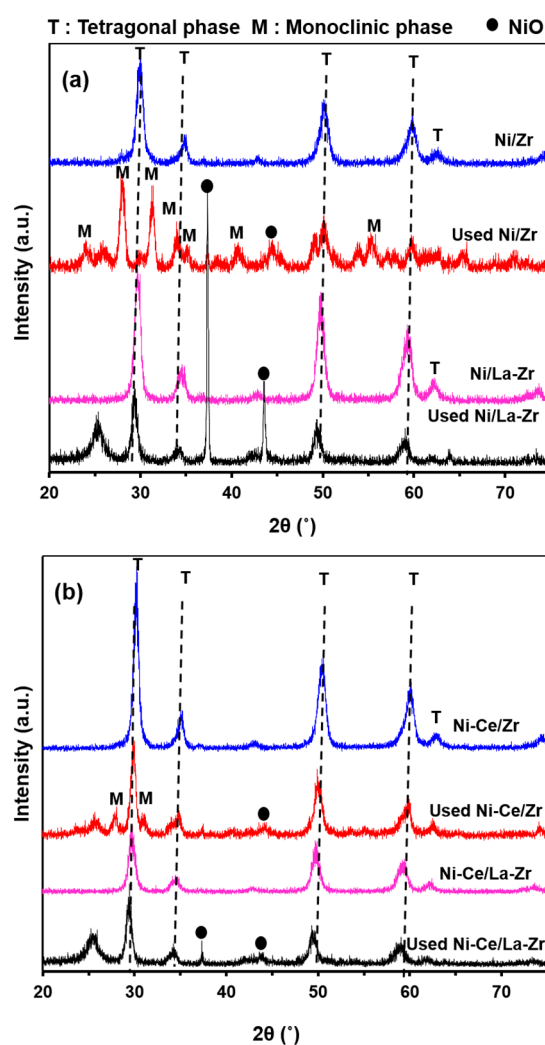


**Figure 1.** X-ray diffraction patterns of fresh and used (a)  $\text{Ni}/x\text{-Zr}$  ( $x = 0, \text{La}_2\text{O}_3$ ) and (b)  $\text{Ni-Ce}/x\text{-Zr}$  catalysts.

According to the literature, monoclinic zirconia ( $m\text{-ZrO}_2$ ) was found at  $2\theta \approx 24.0^\circ, 28.2^\circ, 31.5^\circ, 34.2^\circ, 34.4^\circ, 35.3^\circ$  and  $40.7^\circ$ , while tetragonal zirconia ( $t\text{-ZrO}_2$ ) appeared at  $2\theta \approx 30.0^\circ, 34.8^\circ, 35.1^\circ$ ,

50.0° and 59.4° [24]. Based on this evidence, it can be observed that “pure” Ni/Zr catalyst predominantly consists of *t*-ZrO<sub>2</sub>. After incorporation of La<sub>2</sub>O<sub>3</sub>, the peaks related to *t*-ZrO<sub>2</sub> became sharper and more pronounced. It implies that La<sub>2</sub>O<sub>3</sub> contributed to enhance the stability of the *t*-ZrO<sub>2</sub> phase of the Ni/Zr catalyst. Moreover, it is clear that the crystalline La<sub>2</sub>O<sub>3</sub> phase ( $2\theta = 28^\circ$  and  $49^\circ$ , JCPDS: 01-089-4016) was not individually identified on the diffractograms, indicating that La<sub>2</sub>O<sub>3</sub> was highly dispersed and incorporated into the ZrO<sub>2</sub> lattice. Furthermore, when the Ni/Zr catalyst was promoted using 1% CeO<sub>2</sub> (see Figure 1b), more intense diffraction patterns attributing to *t*-ZrO<sub>2</sub> appeared for the Ni-Ce/Zr catalyst. However, when Ni/La-Zr was promoted by 1% CeO<sub>2</sub>, the intensity of diffraction peaks corresponding to *t*-ZrO<sub>2</sub> was considerably reduced for the Ni-Ce/La-Zr catalyst.

The textural properties of Ni/x-Zr ( $x = 0, \text{La}_2\text{O}_3$ ) and CeO<sub>2</sub> promoted fresh catalysts are shown in Figure 2 and Table 1. It is evident that the incorporation of lanthanum as a ZrO<sub>2</sub> modifier in the catalyst composition led to a significant enhancement of surface area and porosity with respect to the reference Ni/Zr sample.

**Table 1.** Properties and H<sub>2</sub> consumption during reduction of NiO species of fresh Ni/x-Zr and Ni-Ce/x-Zr ( $x = 0, \text{La}_2\text{O}_3$ ) catalysts (calcined at 600 °C).

SAMPLE	BET (m <sup>2</sup> /g)	P.V. (cm <sup>3</sup> /g)	P.D. (nm)	H <sub>2</sub> Consumption (μmol/g)
La-Zr	67	0.247	4.0	-
Ni/Zr	39	0.111	11.3	1049.3
Ni/La-Zr	62	0.246	15.8	814.2
Ni-Ce/Zr	41	0.139	13.3	945.5
Ni-Ce/La-Zr	65	0.242	15.0	782.2

In particular, the Ni/La-Zr sample presented the highest cumulative pore volume (P.V., 0.246 cm<sup>3</sup>/g), accounting for an average pore diameter (P.D.) just smaller than 16 nm. However, the undoped Ni/Zr sample exhibited the lowest extension of surface area (39 m<sup>2</sup>/g) along with the lowest porosity (0.111 cm<sup>3</sup>/g).

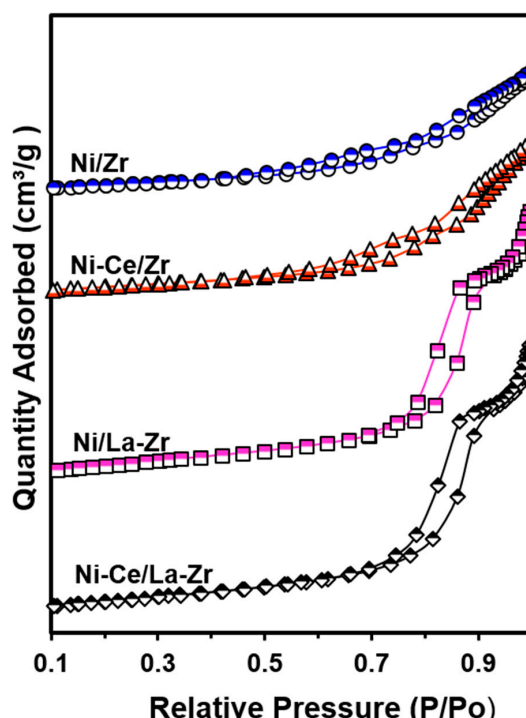


**Figure 2.** N<sub>2</sub> adsorption–desorption isotherms of fresh Ni/x-Zr and Ni-Ce/x-Zr ( $x = 0, \text{La}_2\text{O}_3$ ) catalysts.

Moreover, the  $N_2$  adsorption–desorption branch of the Ni/Zr sample exemplifies a typical type IV isotherm, characteristic for mesoporous solids with a  $H_4$ -type hysteresis loop. The doping of  $ZrO_2$  with  $La_2O_3$  dramatically affected the hysteresis loop, transforming it into a  $H_1$ -type hysteresis loop, associated with a cylindrical pore geometry as well as relatively high uniformity in pore size. Consequently, the  $La_2O_3$  modified catalyst possessed a high surface area and a mesoporous structure. After promotion with 1%  $CeO_2$ , no significant change in the textural properties of the catalysts was observed either in quantitative (see Table 1) or qualitative (see Figure 2) terms.

The reducibility and metal-support interaction of the Ni/Zr system after the support modification was evaluated by TPR analysis. Figure 3 illustrates the reduction profile of Ni/x-Zr ( $x = 0, La_2O_3$ ) and Ni-Ce/x-Zr ( $x = 0, La_2O_3$ ) samples.

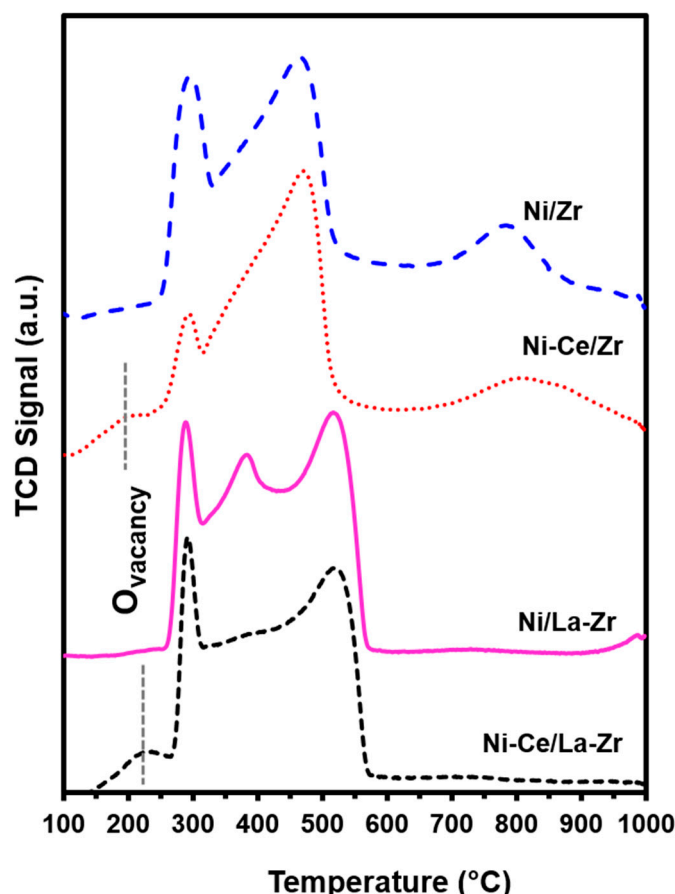


**Figure 3.** TPR profiles of fresh Ni/x-Zr and Ni-Ce/x-Zr ( $x = 0, La_2O_3$ ) catalysts.

It is evident from the TPR profile that the modification of  $ZrO_2$  support by the addition of  $La_2O_3$  has a considerable influence on the reduction profiles, being in all cases characterized by the occurrence of multiple reduction peaks, spanning the range 100–1000 °C, and ascribed to different nickel species with different degrees of interaction with the support. A first reduction peak observed in the range 260–290 °C with a shoulder at some lower temperature in the case of  $CeO_2$  promoted catalysts, may be assigned to the reduction of surface oxygen species [25,26]. The second reduction peak can be referred to the reduction of  $NiO$  grafted onto the support by the weak interaction. The reduction peak at a higher temperature (>750 °C) may be attributed to the development of  $NiO-ZrO_2$  solid solutions [27]. It is interesting to observe that the modification of  $ZrO_2$  with  $La_2O_3$  considerably improved the reduction kinetics, considering that  $NiO$  was completely reduced ( $NiO \rightarrow Ni$ ) below 550 °C owing to the inhibition of formation of  $NiO-ZrO_2$  solid solutions. It implies that the incorporation of  $La_2O_3$  to  $ZrO_2$  had made it feasible to achieve the active metal at some lower temperature accompanied by

the improved dispersion of metallic species. Furthermore, upon  $\text{ZrO}_2$  modification using lanthana, the peaks corresponding to  $\text{NiO-ZrO}_2$  solid solutions seemed to be completely suppressed. It implies that  $\text{La}_2\text{O}_3$  modification also prevents the formation of  $\text{NiO-ZrO}_2$  solid solutions. On the other hand,  $\text{La}_2\text{O}_3$  modification also contributed to enhancing the metal–support interaction, which is evident from the drop in  $\text{H}_2$  consumption from  $\text{Ni/Zr}$  to the  $\text{Ni/La-Zr}$  catalyst by 22% and from  $\text{Ni-Ce/Zr}$  to the  $\text{Ni-Ce/La-Zr}$  catalyst by 17% (Table 1). It is likely that the enhancement in the metal–support interaction is accompanied by the improvement in active phase dispersion. Likewise, Rotgerink et al. [28] also established that the incorporation of  $\text{La}_2\text{O}_3$  to the  $\text{Ni/Zr}$  catalyst upgrades the reducibility and Ni dispersion. Some other studies have also found that the improvement in the reducibility of  $\text{NiO}$  is the outcome of the ability of  $\text{La}_2\text{O}_3$  to disperse Ni metallic species on the  $\text{ZrO}_2$  support [29,30]. After doping by  $\text{CeO}_2$ , the reduction patterns of catalysts had not significantly changed. Furthermore, in the case of the  $\text{Ni-Ce/La-Zr}$  catalyst, a peak centred at 225 °C, corresponding to surface oxygen species, became prominent, which may be the outcome of the synergistic effect of  $\text{CeO}_2$  and  $\text{La}_2\text{O}_3$ . Actually, the  $\text{La}_2\text{O}_3$  lattice is recognized for surface and bulk oxygen vacancies, and their density is associated with the  $\text{La}_2\text{O}_3$  concentration [31].

The quantitative data of  $\text{H}_2$ -TPD measurements are listed in Table 2.

**Table 2.** Data of  $\text{H}_2$ -TPD measurements.

SAMPLE	$\text{H}_2$ uptake ( $\mu\text{mol/g}_{\text{cat}}$ )	MSA <sup>a</sup> ( $\text{m}^2/\text{g}_{\text{cat}}$ )	$D_{\text{Ni}}$ <sup>b</sup> (%)	$d_{\text{Ni}}$ <sup>c</sup> (nm)
Ni/Zr	107.3	8.4	25.2	4.0
Ni/La-Zr	253.3	19.8	59.6	1.7
Ni-Ce/Zr	173.5	13.6	40.8	2.5
Ni-Ce/La-Zr	182.5	14.3	42.9	2.4

<sup>a</sup> Metal surface area. <sup>b</sup> Nickel dispersion. <sup>c</sup> Average Ni particle diameter.

Given the same concentration of Ni in the catalysts, it was observed how the various modifiers of the  $\text{ZrO}_2$  support, as well as the promotion of the active phase with ceria, affect the surface characteristics of the prepared samples. In fact, the “unpromoted”  $\text{Ni/Zr}$  sample exhibited the lowest  $\text{H}_2$  uptake (107.3 mol/g<sub>cat</sub>), accounting for a minor metal surface area ( $8.4 \text{ m}^2/\text{g}_{\text{cat}}$ ) and dispersion (25.2%), as the result of particles not larger than 4 nm generated during preparation. Instead, promotion of carrier oxide by lanthanum oxide positively influenced the  $\text{Ni/Zr}$  system, favouring higher metal surface area and dispersion (16.3–19.8  $\text{m}^2/\text{g}$  and 49.2–59.6%, respectively), as the result of particles with a smaller diameter (1.7–2.1 nm). Regarding the effect of ceria, a promoting effect was markedly evident only on the  $\text{Ni/Zr}$  system, allowing an enhancement both in terms of metal surface area ( $13.6 \text{ m}^2/\text{g}$ ) and nickel dispersion (40.8%). In contrast, it is clearly visible that the  $\text{Ni-Ce/La-Zr}$  sample showed that the surface properties dropped with respect to the sample without Ce (Ni/La-Zr). This suggests that ceria promotion has some inhibiting effect on the  $\text{Ni/La-Zr}$  catalyst.

The basic properties of  $\text{Ni/x-Zr}$  ( $x = 0$ ,  $\text{La}_2\text{O}_3$ ) catalysts were estimated by  $\text{CO}_2$  desorption measurements. Figure 4 illustrates the TPD profiles of the catalysts. It is recognized that the strength of basic sites is determined by the adsorption and desorption peak of  $\text{CO}_2$  in the corresponding temperature range: weak basic sites (50–200 °C), medium/Lewis basic sites (200–400 °C) and strong basic sites (400–650 °C).

The TPD profiles depicted the weak Lewis and moderate Lewis basicity of the reference  $\text{Ni/Zr}$  and  $\text{La}_2\text{O}_3$ -modified samples. It is clearly visible that the  $\text{Ni/Zr}$  catalyst experienced no significant variation in the basic character after  $\text{CeO}_2$  promotion except a rise in basicity in  $\text{La}_2\text{O}_3$  modified catalysts.

XPS analyses were conducted to determine and interpret the chemical state of elements present in the catalysts and the correspondent spectra are illustrated in Figure 5.

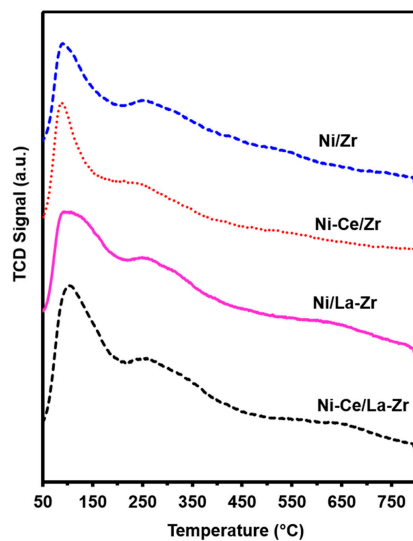


**Figure 4.** Patterns of fresh Ni/x-Zr and Ni-Ce/x-Zr ( $x = 0$ ,  $\text{La}_2\text{O}_3$ ) catalysts.

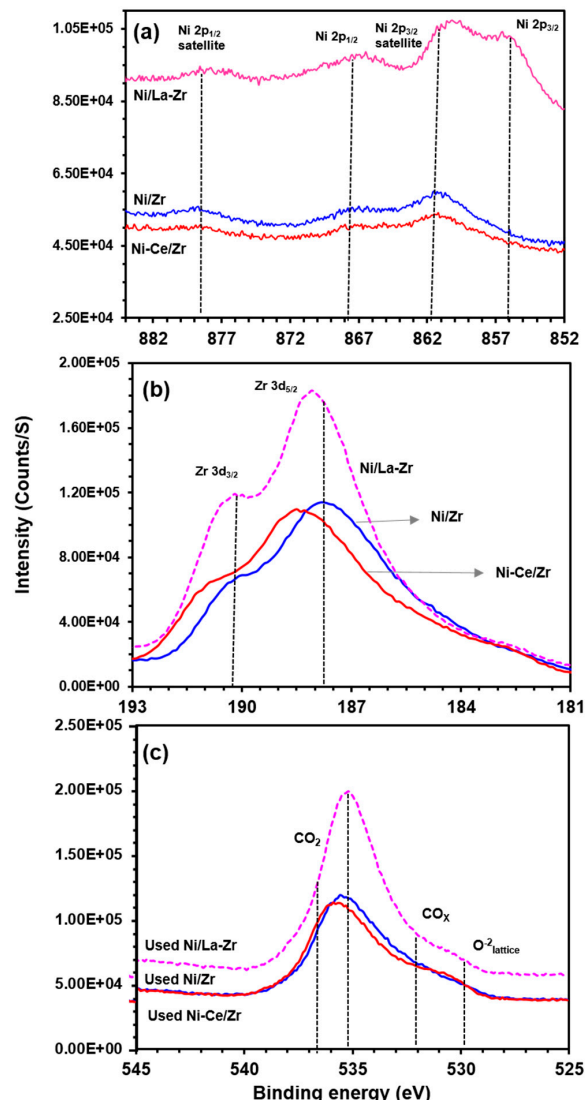


**Figure 5.** Spectra in the “fresh” (a)  $\text{Ni}$  2p, (b)  $\text{Zr}$  3d and “used” (c)  $\text{O}$  1s regions of  $\text{Ni}/\text{La-Zr}$ ,  $\text{Ni}/\text{Zr}$  and  $\text{Ni-Ce}/\text{Zr}$  catalysts.

Ni 2p peaks of all the catalysts Ni/Zr, Ni-Ce/Zr and Ni/La-Zr are presented in Figure 5a. The binding energy of the main Ni 2p peak may be found at 855.6 eV, while the rest of the peaks and satellites are visible at other binding energies. It is apparent from the shape of the main peak ( $\text{Ni } 2\text{p}_{3/2}$ ) that it is the combination of  $\text{Ni}^0$  and  $\text{Ni}^{2+}/\text{Ni}^{3+}$  oxides [32,33]. The Ni 2p spectra of Ni/La-Zr and Ni-Ce/Zr catalysts becomes complicated due to the overlapping of La 3d, Ce 3d, and La MNN Auger peaks. As a result, it gives rise to uncertainty in the quantification of the XPS spectra. Generally, the largest uncertainty is confronted as an outcome of the overlapping of  $\text{Ni } 2\text{p}_{3/2}$  and  $\text{La } 3\text{d}_{3/2}$ . However, in our case, the Ni/La-Zr catalyst was found to have the highest Ni concentration. The Zr 3d peaks of Ni/Zr, Ni/La-Zr and Ni-Ce/Zr catalysts are shown in Figure 5b. Zr  $3\text{d}_{3/2}$  and Zr  $3\text{d}_{5/2}$  can be found at 190.1 eV and 188.2 eV, respectively, for the Ni/Zr catalyst. Upon support modification using  $\text{La}_2\text{O}_3$ , the intensity of the Zr 3d peak significantly increased and it shifted to a higher binding energy. Likewise,  $\text{CeO}_2$  promoted peaks also shifted toward a higher binding energy. The shifting of binding energy to higher values may be attributed to the enhancement of oxygen vacancy as a result of an oxygen deficient state. The phenomenon of shifting of Zr 3d binding energy is related to the large quantity of lattice defects (oxygen vacancies) [34]. The O 1s data for Ni/Zr, Ni-Ce/Zr, Ni/La-Zr, used Ni/Zr and Ni/La-Zr catalysts are illustrated in Figure 5c. The binding energy of O 1s located at 529.6 eV, corresponding to low energy primary oxygen, is consistent for all the catalysts. This peak may be attributed to lattice oxygen ( $\text{O}^{2-}_{\text{lattice}}$ ). The O 1s XPS data also displayed a small amount of  $\text{CO}_x$  species, which implies that  $\text{CO}_x$  species are present as reaction intermediates on the catalyst surface. Consequently, significant variation in chemical states of the catalyst after La incorporation into Ni/Zr implies that support modification using  $\text{La}_2\text{O}_3$  has substantial influence.

## 2.2. Catalytic Activity and Stability

The catalytic behavior of the prepared samples was investigated under dry reforming conditions, in terms of carbon dioxide and methane conversion as a function of time on stream for Ni/x-Zr and Ni-Ce/x-Zr ( $x = 0, \text{La}_2\text{O}_3$ ) catalysts (Figure 6). The effects of  $\text{ZrO}_2$  modification, as well as Ni doping with cerium oxide on the Ni/Zr system, were analyzed. A maximum reaction temperature of 700 °C was chosen, considering that at higher temperature, the formation of encapsulated carbon leads to a rapid deactivation of the system [35,36].

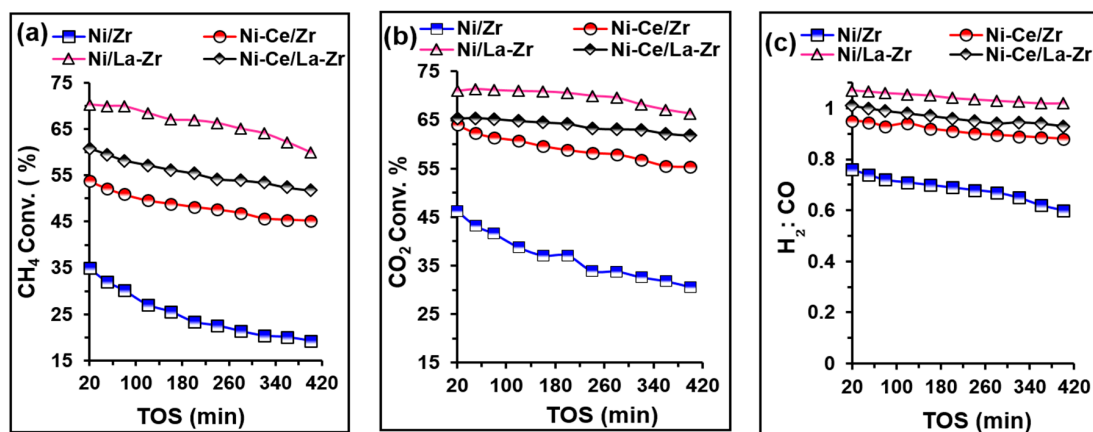


**Figure 6.** (a)  $\text{CH}_4$  and (b)  $\text{CO}_2$  conversion and (c)  $\text{H}_2:\text{CO}$  ratio versus time on stream (TOS) for Ni/x-Zr ( $x = 0, \text{La}_2\text{O}_3$ ) catalysts at  $T_R = 700$  °C; F/W = 133.33 mL/min·g<sub>cat</sub>). Total flow rate = 40 mL/min ( $\text{CH}_4 = 17$  mL/min,  $\text{CO}_2 = 17$  mL/min,  $\text{N}_2 = 6$  mL/min).

It can be seen that not only La modification affects Ni/Zr activity, but also ceria significantly influences the catalytic behavior of the investigated samples. The “reference” Ni/Zr sample exhibited the worst performance, with an initial  $\text{CH}_4$  and  $\text{CO}_2$  conversion of 35 and 46%, respectively, which decreased to 20–30% after only 400 min. After the incorporation of La, the conversion rate of the catalyst samples

was significantly enhanced. Interestingly, the best catalytic performance was obtained by using the La-modified sample, with similar initial values of CH<sub>4</sub> and CO<sub>2</sub> conversion (ca. 70%) and final conversion of 61 (CH<sub>4</sub>) and 67% (CO<sub>2</sub>), accounting for a slightly higher stability in respect to the other samples. Regarding the influence of the CeO<sub>2</sub> promoter, from Figure 6 a net improvement in the activity of the Ni-Ce/Zr sample can be observed, not only in terms of initial conversion values of CH<sub>4</sub> and CO<sub>2</sub> (54 and 64% respectively), but also in terms of stability, considering that after 400 min the CH<sub>4</sub> conversion decreased from 54 to 45%, and CO<sub>2</sub> conversion decreased from 64 to 55%, which were lower with respect to the values recorded in the correspondent catalyst without ceria. Instead, 1% CeO<sub>2</sub> promoter on the Ni phase showed an inhibiting effect on the Ni/La-Zr catalyst, since the activity of the Ni-Ce/La-Zr sample dropped to lower conversion values with respect to the correspondent unpromoted catalyst, by exhibiting a more pronounced decay trend of CH<sub>4</sub> conversion from 61 to 52%. In terms of the H<sub>2</sub>/CO ratio (Figure 6c), a decreasing trend over time on the stream is visible for Ni/Zr, progressively favouring a bit greater formation of CO (Equation (3)) with a final H<sub>2</sub>/CO value of 0.6. However, upon La<sub>2</sub>O<sub>3</sub> modification, an equimolar formation of hydrogen and carbon monoxide with a H<sub>2</sub> / CO ≥ 1 was achieved. On the whole, looking at the properties of the investigated samples, an almost straight-line relationship was found between the initial CO<sub>2</sub> conversion rate and the nickel surface area (see Figure 7). It seems evident that a controlled modification of the carrier structure determines a better surface exposure of the active phase (Ni), and therefore inducing higher CO<sub>2</sub> activation.

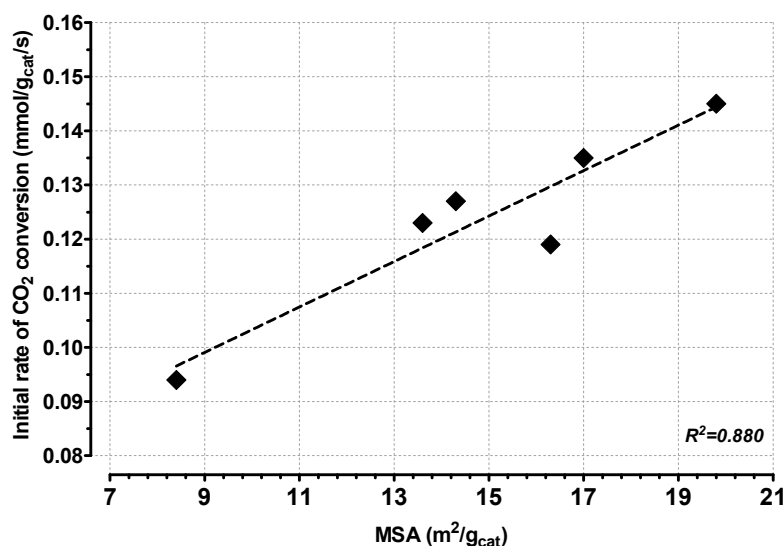


**Figure 7.** Initial rate of CO<sub>2</sub> conversion ( $T_R = 700\text{ }^\circ\text{C} @ 20\text{ min}$ ) as a function of MSA.

The catalyst activity must also be put in direct relation to the catalyst structure, considering that, depending on modification by oxides, ZrO<sub>2</sub> can become a prominently more stable phase. In general, a substantially higher activity is observed when ZrO<sub>2</sub> exists as a tetragonal phase, resulting in appreciably suppressed *m*-ZrO<sub>2</sub> phase even in the used catalysts, like the Ni/La-Zr and Ni-Ce/La-Zr samples (see Figure 1a,b). On the other hand, initially, Ni/Zr and Ni-Ce/Zr had a prominent *t*-ZrO<sub>2</sub> phase, however, upon thermal treatment, tetragonal-to-monoclinic phase transformation occurred.

To better analyze the obtained results, a deactivation factor (DF) was also deduced for all the samples as the ratio between the loss of activity calculated between the initial (20 min on stream) and final (400 min on stream) time and the initial conversion value of CH<sub>4</sub>. From Figure 8, it is evident that the incorporation of La<sub>2</sub>O<sub>3</sub> considerably improves the catalyst stability of the Ni/Zr system, as the deactivation factor decreased from 44% to 22%, with a lower net drop of the activity in respect of the initial time under the same experimental conditions. Moreover, the addition of ceria leads to a further improvement of the catalytic stability for both the undoped Ni/Zr and Ni/La-Zr samples, yielding the smallest loss of activity during time (< 12%) in the Ni-Ce/La-Zr sample.

To investigate the phase analysis following the catalytic treatment, post reaction XRD of the catalysts was performed (Figure 1). It was revealed that the thermal treatment had a profound influence on the phase transformation. For instance, used Ni/Zr catalyst found to have severe lattice distortion and *t*-ZrO<sub>2</sub> had significantly diminished and transformed into *m*-ZrO<sub>2</sub>. Likewise, even CeO<sub>2</sub> promotion to Ni/Zr catalyst was not able to completely preserve the *t*-ZrO<sub>2</sub>. However, upon support modification using La<sub>2</sub>O<sub>3</sub>, the *t*-ZrO<sub>2</sub> phase was perfectly retained with no appearance of *m*-ZrO<sub>2</sub>. It implies that La<sub>2</sub>O<sub>3</sub> incorporation has a significant contribution in stabilizing the *t*-ZrO<sub>2</sub> and achieving the 100% rise in catalytic activity. Similarly, used Ni-Ce/La-Zr also prevented the tetragonal-to-monoclinic transformation and pure *t*-ZrO<sub>2</sub> was preserved.

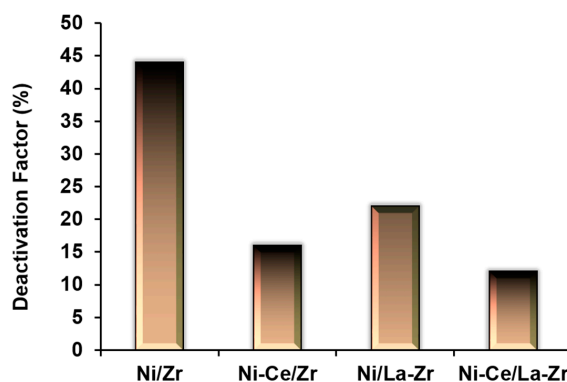


**Figure 8.** Deactivation factor (DF) of Ni/x-Zr ( $x = 0, \text{La}_2\text{O}_3$ ) catalysts, calculated as: [(Initial CH<sub>4</sub> conversion – final CH<sub>4</sub> conversion)/initial conversion of CH<sub>4</sub>] (Initial = 20 min; Final = 400 min at  $T_R = 700^\circ\text{C}$ ).

As a main possible reason for the decay of activity during time, it was obviously necessary to consider the coke formation over the different samples, as it is known that the amount and typology of coke is also influenced by the catalyst properties. On this account, temperature programmed oxidation (TPO) ceria promoted and unpromoted Ni/x-ZrO<sub>2</sub> ( $0, \text{La}_2\text{O}_3$ ) catalysts were conducted to determine the type of the deposited carbon during the CO<sub>2</sub> reforming reactions. The TPO peaks are illustrated in Figure 9a.

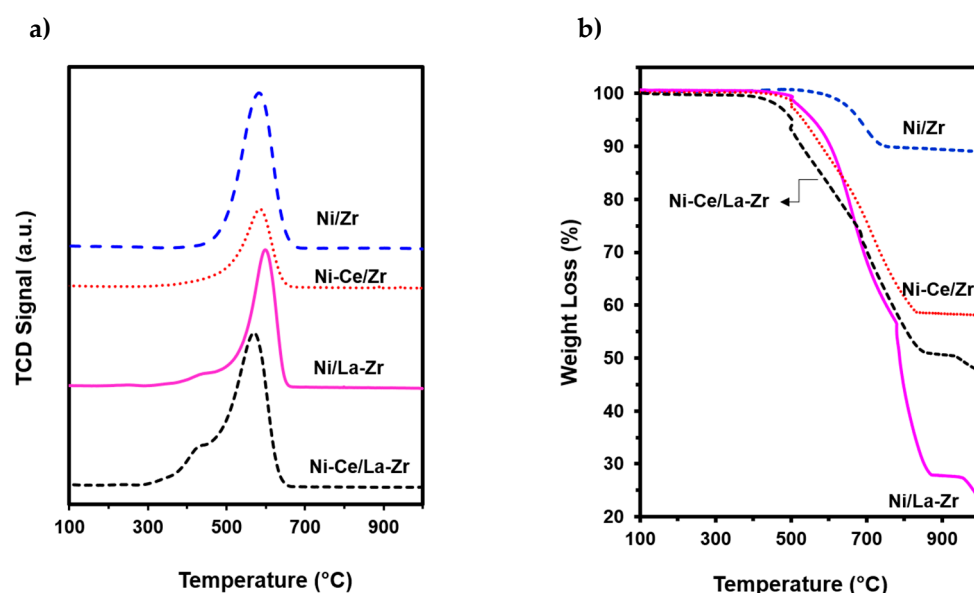


**Figure 9.** (a) TPO profiles of “spent” Ni/x-Zr and Ni-Ce/x-Zr ( $x = 0, \text{La}_2\text{O}_3$ ) catalysts after reaction at  $T_R = 700^\circ\text{C}$  and (b) TGA profiles of “spent” Ni/x-Zr and Ni-Ce/x-Zr ( $x = 0, \text{La}_2\text{O}_3$ ) catalysts after reaction at  $T_R = 700^\circ\text{C}$ .

The major peak in each profile is positioned around 585 °C, suggesting the presence of carbon nanotubes (CNTs). TGA analysis of spent catalysts was performed on reference and promoted Ni/Zr catalysts (Figure 9b) to quantify the amount of deposited carbon. It was found that no significant weight loss occurs in the case of a pure catalyst, indicating that a low amount of carbon was deposited during the reaction. On the contrary, La-modified catalysts presented a higher weight loss. After CeO<sub>2</sub> promotion, TGA profiles illustrate that the amount of accumulated carbon on the catalyst surface had considerably reduced. Moreover, the corresponding peaks negatively shifted, implying that the type of carbon material formed, is less stable, and burnt at a relatively lower temperature. It implies that carbon nanotubes (CNTs) mainly formed after CeO<sub>2</sub> promotion, and are easily burnt and affect catalyst deactivation less [7,37–39].

Figures 10 and 11 show the TEM images of ceria promoted and unpromoted Ni/x-ZrO<sub>2</sub> (0, La<sub>2</sub>O<sub>3</sub>) catalysts.

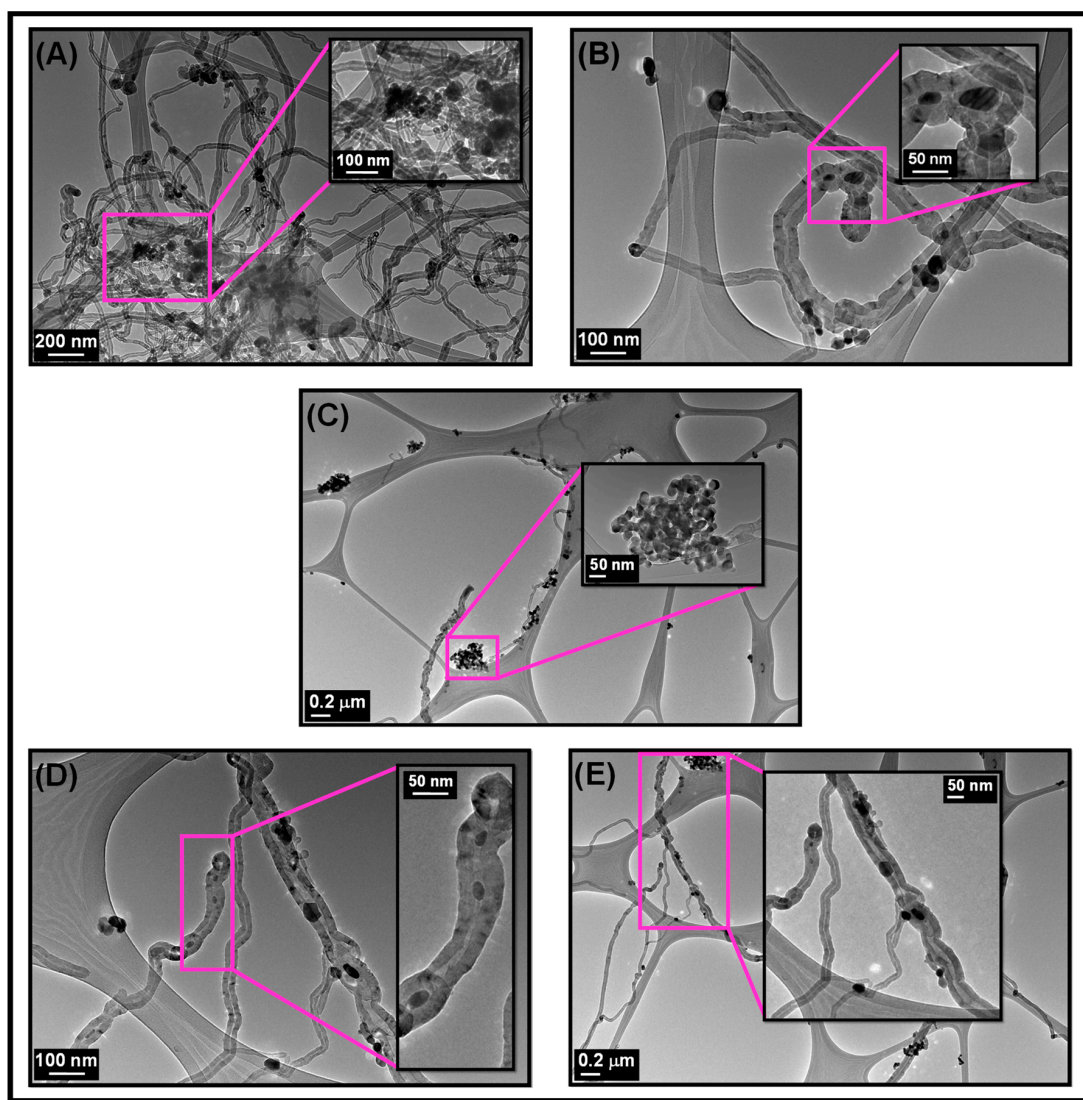


**Figure 10.** Micrographs of the “spent” Ni/Zr sample ( $T_R = 700$  °C; reaction time = 400 min): (A) cluster of CNTs; (B) metal sintering; (C) encapsulation of metal species; (D) and (E) metal particles captured inside CNTs.

It can be seen that the majority of the deposited carbon on the Ni/ZrO<sub>2</sub> surface, after the catalytic reaction, is of a filamentous nature, and a tangle of carbon nanotubes (CNTs) is clearly visible (Figure 10A), while the rest of the carbon is of the encapsulating type. It is clear that several particles

were encapsulated due to the carbon formation on Ni surface (Figure 10B). Ni/ZrO<sub>2</sub> catalysts also undergo sintering, therefore accumulation of metallic species can be seen (Figure 10C). Conspicuously, metal particles varying in size in the range 2–9 nm were entrapped inside the CNTs (Figure 10D,E), which may be another reason for the lower activity of the pristine catalyst.

When the pristine catalyst Ni/Zr was modified with La<sub>2</sub>O<sub>3</sub>, morphological investigation revealed the formation of multiwall carbon nanotubes (MWCNTs). The average external diameter of MWCNTs was found to be 28 nm, whereas the metallic species were positioned together in the interior as well as on the exterior of MWCNTs (Figure 11A). It seems that the incorporation of La<sub>2</sub>O<sub>3</sub> had no influence in controlling the sintering of metallic particles (Figure 11B). The Ni particles at the tip of the CNTs clearly demonstrated that Ni particles not strongly anchored to the catalyst support formed filaments with a mechanism that included the diffusion of elementary C through the Ni and precipitation on the back side of the particle with consequent formation of the filament. In this case, Ni continues to be active for dry reforming [40–42]. Furthermore, when the Ni/ZrO<sub>2</sub> catalyst was promoted using CeO<sub>2</sub>, the situation escalated because the rate of sintering was significantly enhanced upon CeO<sub>2</sub> promotion (Figure 11C), which may justify the deteriorating activity of the Ni-Ce/La-Zr catalyst.

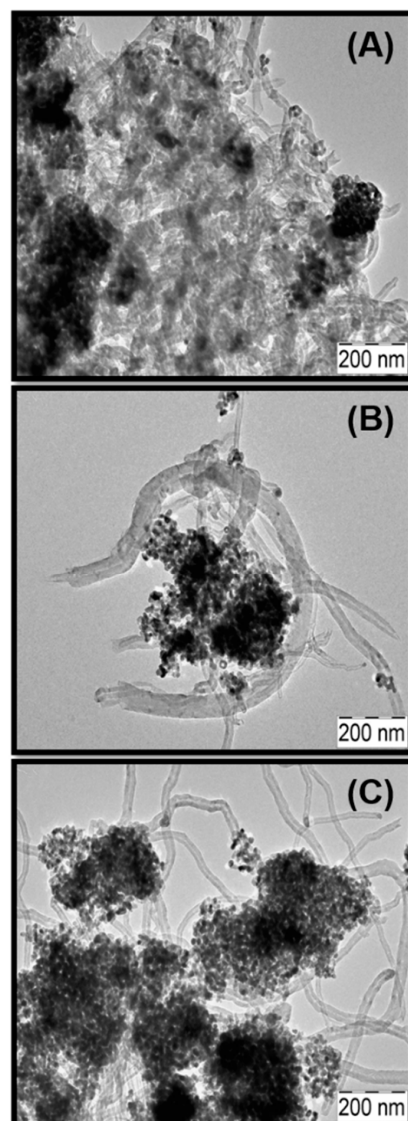


**Figure 11.** Micrographs of the “spent” Ni/La-Zr sample ( $T_R = 700\text{ }^{\circ}\text{C}$ ; reaction time = 400 min): (A) CNTs over catalyst surface; (B) metal particles sintering; (C) influence of Ce addition.

### 3. Materials and Methods

#### 3.1. Catalyst Preparation

In this experimental work an incipient wet-impregnation technique was used to prepare the desired catalysts for the dry reforming of methane. The supports (zirconium oxide and modified zirconium oxide with  $\text{La}_2\text{O}_3$ ) along with the active metal obtained from the precursor of Ni nitrate [ $\text{Ni}(\text{NO}_3)_2 \cdot 6\text{H}_2\text{O}$ ; 99.9% purity] were dissolved in distilled water. The amount of Ni used in the catalyst was 5 wt%. The solution was kept heated at 90 °C under stirring for 3 h. Later, impregnated catalysts were heated up to 120 °C overnight for drying and then subjected to calcination at 600 °C for 3 h. The  $\text{Ce}(\text{NO}_3)_3 \cdot 6\text{H}_2\text{O}$  promoted catalysts with 1 wt% were prepared by co-impregnation of the nitrate salts of the promoter and active metal with support using the same procedure mentioned above. The solution was kept heated at 90 °C under stirring for 3 h. Later, impregnated catalysts were heated up to 120 °C overnight for drying and then subjected to calcination at 600 °C for 3 h. The commercial samples of the support were obtained from KIGAKU DAIICHI KOGYO CO.; LTD, Osaka, Japan. We are grateful to the company for providing us with free samples.

#### 3.2. Catalytic Testing

Dry reforming of  $\text{CH}_4$  experiments over  $\text{Ni}/\text{ZrO}_2$  catalysts were performed at 700 °C and at atmospheric pressure in a vertical stainless steel fixed-bed tubular (i.d., 9.1 mm; length, 0.3 m) micro-reactor (PID Eng & Tech micro activity reference, Madrid, Spain). Activity tests were performed using 0.1 g of a catalyst placed in a quartz reactor between two quartz wool beds. A K-type stainless steel sheathed thermocouple, placed axially at the center of the catalyst bed, measured the temperature during the reaction. Prior to each test, the catalysts were activated under a continuous flow of  $\text{H}_2$  (20 mL/min) for 1 h at 600 °C. Experiments were carried out using a feed gas mixture ( $\text{CH}_4$ ,  $\text{CO}_2$  and  $\text{N}_2$ ) at the ratio 6/6/1 and overall gas flow rate of 65 mL/min (space velocity: 39,000 mL/h.g<sub>cat</sub>). The outlet gas composition was analyzed by on-line gas chromatography (Shimadzu 2014, Kyoto, Japan) fitted out with a thermal conductivity detector (TCD). The  $\text{CH}_4$  conversion and hydrogen yield were determined using the following formulae:

$$\text{CH}_4 \text{ conversion}(\%) = \frac{(\text{CH}_4_{\text{in}} - \text{CH}_4_{\text{out}})}{\text{CH}_4_{\text{in}}} * 100 \quad (5)$$

$$\text{H}_2 \text{ yield}(\%) = \frac{(\text{H}_2_{\text{out}})}{2 * \text{CH}_4_{\text{in}}} * 100 \quad (6)$$

#### 3.3. Catalyst Characterization

##### 3.3.1. XRD Characterization

Rigaku (Miniflex) diffractometer (Rigaku Corporation, Dover, DE, USA), with a Cu K $\alpha$  X-ray radiation working at 40 kV and 40 mA, was used to investigate the structure of the catalysts before and after the reaction. The scanning 2 $\theta$  range and steps were 10–85° and 0.02° respectively. The raw data file of the instrument was evaluated by X'Pert high score plus software (version 2.1, Panalytical, Malvern, UK). Different phases with their scores were corresponded with the JCPDS data bank.

##### 3.3.2. N<sub>2</sub> Physisorption

The specific surface area and distribution of pore size of the catalysts were obtained using Micromeritics Tristar II 3020 surface area and porosity analyzer. The pore size distribution was calculated by BJH method.

### 3.3.3. Temperature Programmed Reduction (TPR)

The TPR measurements were performed using Micromeritics Auto Chem II apparatus (Micromeritics, Atlanta, GA, USA). The sample (70 mg) was charged in the TPR cell and flushed with argon at 150 °C for 30 min. Then the sample temperature was reduced to 25 °C. Finally, the furnace temperature was heated to 1000 °C at 10 °C/min ramp at a 40 mL/min flow rate with a H<sub>2</sub>/Ar mixture (10:90 vol.%). A thermal conductivity detector (TCD) was used to follow the signals of H<sub>2</sub> consumption.

### 3.3.4. H<sub>2</sub> Temperature-Programmed Desorption

To evaluate metal surface area (MSA), and surface average nickel particle size (d<sub>Ni</sub>) of the investigated catalysts, H<sub>2</sub>-TPD measurements in the range 20–900 °C ( $\beta = 10\text{ }^{\circ}\text{C}/\text{min}$ ) were carried out at atmospheric pressure by using a linear quartz micro-reactor (i.d., 4 mm) flowing Ar as carrier gas at 50 stp cm<sup>3</sup>/min. Before measurements, a catalyst sample (50–100 mg) was reduced for half-an hour in flowing H<sub>2</sub> (25 stp cm<sup>3</sup>/min) at 600 °C. Thereafter, the sample was cooled in flowing H<sub>2</sub> to room temperature and then hydrogen was shut off and the sample was purged by the carrier stream until baseline stabilization ( $\approx 20$  min). Assuming a chemisorption stoichiometry H<sub>2</sub>:Ni<sub>surf</sub> = 1:2 and a spherical shape of the metal particle, the following equations were applied:

$$\text{MSA} (\text{m}^2/\text{g}_{\text{cat}}) = 2 \cdot X_{\text{H}_2} \cdot N_{\text{Av}} / \sigma_{\text{Ni}} \quad (7)$$

$$d_{\text{Ni}} (\text{nm}) = 6000 \cdot (C_{\text{Ni}}/100) / (\rho_{\text{Ni}} \cdot \text{MSA}) \quad (8)$$

where “X<sub>H<sub>2</sub></sub>” is the H<sub>2</sub> uptake (mol/g<sub>cat</sub>), “N<sub>Av</sub>” is Avogadro’s number, “σ<sub>Ni</sub>” represents the concentration of surface atoms ( $1.54 \times 10^{19}$  at/m<sup>2</sup> for Ni), “C<sub>Ni</sub>” is the metal loading (wt%), while “ρ<sub>Ni</sub>” is the metal density (8.9 g/cm<sup>3</sup> for Ni).

### 3.3.5. CO<sub>2</sub> Temperature-Programmed Desorption (CO<sub>2</sub>-TPD)

The CO<sub>2</sub> temperature-programmed desorption (TPD) was carried out using a Chemisorption Analyzer (Micromeritics Autochem II apparatus, Micromeritics, Atlanta, GA, USA). The catalyst (50 mg) was reduced at 600 °C for 1 h under He flow (30 mL/min) and then cooled to 50 °C. The CO<sub>2</sub> flow was kept for 60 min, and the sample was then flushed with He to take away any physisorbed CO<sub>2</sub>. The desorption profile of the catalysts were recorded by ramping the temperature at a rate of 10 °C/min, while temperature was then linearly increased up to 800 °C. The CO<sub>2</sub> concentration in the output stream was measured with a thermal conductivity detector, and the areas under the peaks were used to determine the amount of desorbed CO<sub>2</sub> during TPD.

### 3.3.6. Thermo-Gravimetric Analysis (TGA)

The analysis of carbonaceous material deposition post reaction over the catalyst’s surface was quantitatively performed using the TGA-15 SHIMADZU analyzer (Shimadzu, Kyoto, Japan) under an air atmosphere. The spent catalyst (10–15 mg) was heated from room temperature to 1000 °C at a heating rate of 20 °C/min and the loss of weight was measured.

### 3.3.7. TEM Characterization

TEM measurements of the used samples were accomplished on a 120 kV JEOL JEM-2100F transmission electron microscope (JEOL, Peabody, MA, USA).

### 3.3.8. XPS Analysis

X-ray photoelectron spectroscopy (XPS) spectra were recorded on an Omicron Nanotechnology (ELS5000) spectrometer with a monochromatic Al source. X-ray was employed using a flood gun with a spot size of radius  $\sim 400\text{ }\mu\text{m}$ . Survey scanning was acquired from –10 to 1350 eV with energy steps of 1 eV, while employing a pass energy of 200 eV. The number of scans was four with a dwell time

of 10 ms. Similarly, a slow scan was conducted for the element using a pass energy of a 50 eV and the number of scans was four with a dwell time of 10 ms. The charging effects were corrected by adjusting the binding energy of the C 1s peak from adventitious carbon to 285 eV. The characterization experiments were carried out for fresh (before reaction) and used (after reaction) samples.

#### 4. Conclusions

A high surface area  $\text{ZrO}_2$  supported Ni system was prepared using an incipient wet-impregnation method and then modified by heteroatom oxides, like  $\text{La}_2\text{O}_3$ , and the influence of ceria doping in dry reforming of  $\text{CH}_4$  at 700 °C was also assessed. It is worthwhile highlighting that the reduction properties of the catalysts were significantly enhanced upon  $\text{La}_2\text{O}_3$  modification.  $\text{La}_2\text{O}_3$  modification suppressed the formation of  $\text{NiO-ZrO}_2$  solid solutions, with a complete reduction of the active phase at temperatures below 750 °C. Furthermore,  $\text{La}_2\text{O}_3$  modification also contributed to enhancing the metal-support interaction and active phase dispersion. However, the weak-medium basicity of all modified catalyst samples were substantially unchanged after Ce-promotion. Phase analysis revealed that the  $t\text{-ZrO}_2$  phase of the Ni/Zr catalyst had almost completely transformed into the  $m\text{-ZrO}_2$  phase after thermal treatment. However, when  $\text{La}_2\text{O}_3$  incorporated into the  $\text{ZrO}_2$  support, the  $t\text{-ZrO}_2$  phase was protected and prominently stabilized, leading to a superior catalytic performance. Interestingly,  $\text{CH}_4$  conversion increased to 2x, and  $\text{CO}_2$  conversion to 1.5x, that of pristine Ni/ $\text{ZrO}_2$ . However, when the modified catalysts were promoted by  $\text{CeO}_2$ , a decline in catalytic activity was observed in the case of the Ni-Ce/La-Zr catalyst. Eventually, it was revealed that the high activity of  $\text{La}_2\text{O}_3$  modified catalysts was achieved by protecting the stability of the  $t\text{-ZrO}_2$  phase.

**Author Contributions:** A.S.-F., Y.A., A.A.I., S.O.K. and A.H.F. synthesized the catalysts, performed all the experiments and characterization tests and wrote the manuscript. F.F., A.A. and G.B. performed the characterization tests for  $\text{CO}_2$ ,  $\text{H}_2\text{-TPD}$ , XPS and TEM, and proofread the manuscript. A.E.A. contributed to the analysis of the data and proofread the manuscript.

**Funding:** The authors would like to express their sincere appreciation to the Deanship of Scientific Research at King Saud University for funding this research project (No. RGP-1435-078).

**Acknowledgments:** The authors would like to extend their sincere appreciation to the Deanship of Scientific Research at King Saud University for its funding this research group No. (RGP-1435-078).

**Conflicts of Interest:** The authors declare no conflict of interest.

#### References

- Pan, X.; Fan, Z.; Chen, W.; Ding, Y.; Luo, H.; Bao, X. Enhanced ethanol production inside carbon-nanotube reactors containing catalytic particles. *Nat. Mat.* **2007**, *6*, 507–511. [[CrossRef](#)] [[PubMed](#)]
- Hamza Fakieha, A.; Arafat, Y.; Aidid Ibrahim, A.; Shaikh, H.; Atia, H.; Elhag Abasaeed, A.; Armbruster, U.; Sadeq Al-Fatesh, A. Highly Selective Syngas/ $\text{H}_2$  Production via Partial Oxidation of  $\text{CH}_4$  Using (Ni, Co and Ni-Co)/ $\text{ZrO}_2\text{-Al}_2\text{O}_3$  Catalysts: Influence of Calcination Temperature. *Processes* **2019**, *7*, 141. [[CrossRef](#)]
- Gao, X.Y.; Hidajat, K.; Kawi, S. Facile synthesis of Ni/ $\text{SiO}_2$  catalyst by sequential hydrogen/air treatment: A superior anti-coking catalyst for dry reforming of methane. *J. CO<sub>2</sub> Util.* **2016**, *15*, 146–153. [[CrossRef](#)]
- Xu, Y.; Lin, Q.; Liu, B.; Jiang, F.; Xu, Y.; Liu, X. A Facile Fabrication of Supported Ni/ $\text{SiO}_2$  Catalysts for Dry Reforming of Methane with Remarkably Enhanced Catalytic Performance. *Catalysts* **2019**, *9*, 183. [[CrossRef](#)]
- Karam, L.; Casale, S.; El Zakhem, H.; El Hassan, N. Tuning the properties of nickel nanoparticles inside SBA-15 mesopores for enhanced stability in methane reforming. *J. CO<sub>2</sub> Util.* **2017**, *17*, 119–124. [[CrossRef](#)]
- El Hassan, N.; Kaydouh, M.; Geagea, H.; El Zein, H.; Jabbour, K.; Casale, S.; El Zakhem, H.; Massiani, P. Low temperature dry reforming of methane on rhodium and cobalt based catalysts: Active phase stabilization by confinement in mesoporous SBA-15. *Appl. Catal. A Gen.* **2016**, *520*, 114–121. [[CrossRef](#)]
- Al-Fatesh, A.S.; Arafat, Y.; Atia, H.; Ibrahim, A.A.; Ha, Q.L.M.; Schneider, M.; M-Pohl, M.; Fakieha, A.H.  $\text{CO}_2$ -reforming of methane to produce syngas over Co-Ni/SBA-15 catalyst: Effect of support modifiers (Mg, La and Sc) on catalytic stability. *J. CO<sub>2</sub> Util.* **2017**, *21*, 395–404. [[CrossRef](#)]
- Moradi, G.R.; Rahmanzadeh, M.; Khosravian, F. The effects of partial substitution of Ni by Zn in  $\text{LaNiO}_3$  perovskite catalyst form ethane dry reforming. *J. CO<sub>2</sub> Util.* **2014**, *6*, 7–11. [[CrossRef](#)]

9. Kambolis, A.; Matralis, H.; Trovarelli, A.; Papadopoulou, C. Ni/CeO<sub>2</sub>-ZrO<sub>2</sub> catalysts for the dry reforming of methane. *Appl. Catal. A* **2010**, *377*, 16–26. [[CrossRef](#)]
10. Lemonidou, A.A.; Vasalos, I.A. Carbon dioxide reforming of methane over 5 wt.% Ni/CaO-Al<sub>2</sub>O<sub>3</sub> catalyst. *Appl. Catal. A* **2002**, *228*, 227–235. [[CrossRef](#)]
11. Han, J.W.; Park, J.S.; Choi, M.S.; Lee, H. Uncoupling the size and support effects of Ni catalysts for dry reforming of methane. *Appl. Catal. B* **2017**, *203*, 625–632. [[CrossRef](#)]
12. Świrk, K.; Gálvez, M.E.; Motak, M.; Grzybek, T.; Rønning, M.; Da Costa, P. Dry reforming of methane over Zr- and Y-modified Ni/Mg/Al double-layered hydroxides. *Catal. Commun.* **2018**, *117*, 26–32.
13. Sarkar, D.; Adak, S.; Chu, M.; Cho, S.; Mitra, N. Influence of ZrO<sub>2</sub> on the thermo-mechanical response of nano-ZTA. *Ceram. Int.* **2007**, *33*, 255–261. [[CrossRef](#)]
14. Lercher, J.; Bitter, J.; Hally, W.; Niessen, W.; Seshan, K. Design of stable catalysts for methane-carbon dioxide reforming. *Studies Surf. Sci. Catal.* **1996**, *101*, 463–472.
15. Li, X.; Chang, J.; Park, S. Carbon as an intermediate during the carbon dioxide reforming of methane over zirconia-supported high nickel loading catalysts. *Chem. Lett.* **1999**, *10*, 1099–1100. [[CrossRef](#)]
16. Chuah, G.K.; Liu, S.H.; Jaenicke, S.; Li, J. High surface area zirconia by digestion of zirconium propoxide at different pH. *Microporous Mesoporous Mat.* **2000**, *39*, 381–392. [[CrossRef](#)]
17. Jaenicke, S.; Chuah, G.K.; Raju, V.; Nie, Y.T. Structural and Morphological Control in the Preparation of High Surface Area Zirconia. *Catal. Surv. Asia* **2008**, *12*, 153–169. [[CrossRef](#)]
18. Fan, M.-S.; Abdullah, A.Z.; Bhatia, S. Utilization of greenhouse gases through carbon dioxide reforming of methane over Ni-Co/MgO-ZrO<sub>2</sub>: preparation, characterization and activity studies. *Appl. Catal. B* **2010**, *100*, 365–377. [[CrossRef](#)]
19. Yamasaki, M.; Habazaki, H.; Asami, K.; Izumiya, K.; Hashimoto, K. Effect of tetragonal ZrO<sub>2</sub> on the catalytic activity of Ni/ZrO<sub>2</sub> catalyst prepared from amorphous Ni-Zr alloys. *Catal. Commun.* **2006**, *7*, 24–28. [[CrossRef](#)]
20. Rezaei, M.; Alavi, S.M.; Sahebdelfar, S.; Yan, Z.-F. A highly stable catalyst in methane reforming with carbon dioxide. *Scripta Materialia* **2009**, *61*, 173–176. [[CrossRef](#)]
21. Choque, V.; de la Piscina, P.R.; Molyneux, D.; Homs, N. Ruthenium supported on new TiO<sub>2</sub>-ZrO<sub>2</sub> systems as catalysts for the partial oxidation of methane. *Catal. Today* **2010**, *149*, 248–253. [[CrossRef](#)]
22. Verykios, X.E. Catalytic dry reforming of natural gas for the production of chemicals and hydrogen. *Int. J. Hydrogen Energy* **2003**, *28*, 1045–1063. [[CrossRef](#)]
23. Slagtern, A.; Schuurman, Y.; Leclercq, C.; Verykios, X.; Mirodatos, C. Specific features concerning the mechanism of methane reforming by carbon dioxide over Ni/La<sub>2</sub>O<sub>3</sub> catalyst. *J. Catal.* **1997**, *172*, 118–126. [[CrossRef](#)]
24. Titus, J.; Roussiere, T.; Wasserschaff, G.; Schunk, S.; Milanov, A.; Schwab, E.; Wagner, G.; Oeckler, O.; Gläser, R. Dry reforming of methane with carbon dioxide over NiO-MgO-ZrO<sub>2</sub>. *Catal. Today* **2016**, *270*, 68–75. [[CrossRef](#)]
25. Ay, H.; Üner, D. Dry reforming of methane over CeO<sub>2</sub> supported Ni, Co and Ni-Co catalysts. *Appl. Catal. B* **2015**, *179*, 128–138. [[CrossRef](#)]
26. Chen, J.; Zhang, X.; Arandiyani, H.; Peng, Y.; Chang, H.; Li, J. Low temperature complete combustion of methane over cobalt chromium oxides catalysts. *Catal. Today* **2013**, *201*, 12–18. [[CrossRef](#)]
27. Goula, M.A.; Charisiou, N.D.; Siakavelas, G.; Tzounis, L.; Tsiaouassis, I.; Panagiotopoulou, P.; Goula, G.; Yentekakis, I.V. Syngas production via the biogas dry reforming reaction over Ni supported on zirconia modified with CeO<sub>2</sub> or La<sub>2</sub>O<sub>3</sub> catalysts. *Int. J. Hydrogen Energy* **2017**, *42*, 13724–13740.
28. Rotgerink, H.L.; Paalman, R.; Van Ommen, J.; Ross, J. Studies on the promotion of nickel—alumina coprecipitated catalysts: II. Lanthanum oxide. *Appl. Catal.* **1988**, *45*, 257–280. [[CrossRef](#)]
29. Wang, S.; Lu, G.; Millar, G.J. Carbon dioxide reforming of methane to produce synthesis gas over metal-supported catalysts: state of the art. *Energy Fuels* **1996**, *10*, 896–904. [[CrossRef](#)]
30. Kumar, P.; Sun, Y.; Idem, R.O. Comparative Study of Ni-based Mixed Oxide Catalyst for Carbon Dioxide Reforming of Methane. *Energy Fuels* **2008**, *22*, 3575–3582. [[CrossRef](#)]
31. Huang, S.J.; Walters, A.B.; Vannice, M.A. TPD, TPR and DRIFTS studies of adsorption and reduction of NO on La<sub>2</sub>O<sub>3</sub> dispersed on Al<sub>2</sub>O<sub>3</sub>. *Appl. Catal. B* **2000**, *26*, 101–118. [[CrossRef](#)]
32. Grosvenor, A.P.; Biesinger, M.C.; Smart, R.S.C.; McIntyre, N.S. New interpretations of XPS spectra of nickel metal and oxides. *Surf. Sci.* **2006**, *600*, 1771–1779. [[CrossRef](#)]

33. Charisiou, N.D.; Siakavelas, G.; Tzounis, L.; Sebastian, V.; Monzon, A.; Baker, M.A.; Hinder, S.J.; Polychronopoulou, K.; Yentekakis, I.V.; Goula, M.A. An in depth investigation of deactivation through carbon formation during the biogas dry reforming reaction for Ni supported on modified with CeO<sub>2</sub> and La<sub>2</sub>O<sub>3</sub> zirconia catalysts. *Int. J. Hydrogen Energy* **2018**, *43*, 18955–18976. [[CrossRef](#)]
34. Liu, G.; Liu, A.; Meng, Y.; Shan, F.; Shin, B.; Lee, W.; Cho, C. Annealing dependence of solution-processed ultra-thin ZrO<sub>x</sub> films for gate dielectric applications. *J. Nanosci. Nanotechnol.* **2015**, *15*, 2185–2191. [[CrossRef](#)]
35. Italiano, G.; Delia, A.; Espro, C.; Bonura, G.; Frusteri, F. Methane decomposition over Co thin layer supported catalysts to produce hydrogen for fuel cell. *Int. J. Hydrogen Energy* **2010**, *35*, 11568–11575. [[CrossRef](#)]
36. Frusteri, F.; Italiano, G.; Espro, C.; Cannilla, C.; Bonura, G. H<sub>2</sub> production by methane decomposition: Catalytic and technological aspects. *Int. J. Hydrogen Energy* **2012**, *37*, 16367–16374. [[CrossRef](#)]
37. Frusteri, F.; Frontera, P.; Modafferi, V.; Bonura, G.; Bottari, M.; Siracusano, S.; Antonucci, P.L. Catalytic features of Ni/Ba–Ce0.9–Y0.1 catalyst to produce hydrogen for PCFCs by methane reforming. *Int. J. Hydrogen Energy* **2010**, *35*, 11661–11668.
38. Frontera, P.; Macario, A.; Monforte, G.; Bonura, G.; Ferraro, M.; Dispenza, G.; Antonucci, V.; Aricò, A.S.; Antonucci, P.L. The role of Gadolinia Doped Ceria support on the promotion of CO<sub>2</sub>methanation over Ni and NiFe catalysts. *Int. J. Hydrogen Energy* **2017**, *42*, 26828–26842. [[CrossRef](#)]
39. Al-Fatesh, A.S.; Arafat, Y.; Ibrahim, A.A.; Atia, H.; Fakieha, A.H.; Armbruster, U.; Abasaeed, A.E.; Frusteri, F. Evaluation of Co-Ni/Sc-SBA-15 as a novel coke resistant catalyst for syngas production via CO<sub>2</sub> reforming of methane. *Appl. Catal. A* **2018**, *567*, 102–111. [[CrossRef](#)]
40. Bonura, G.; Di Blasi, O.; Spadaro, L.; Arena, F.; Frusteri, F. A basic assessment of the reactivity of Ni catalysts in the decomposition of methane for the production of “CO<sub>x</sub>-free” hydrogen for fuel cells application. *Catal. Today* **2006**, *116*, 298–303. [[CrossRef](#)]
41. Frusteri, F.; Spadaro, L.; Arena, F.; Chuvilin, A. TEM evidence for factors affecting the genesis of carbon species on bare and K-promoted Ni/MgO catalysts during the dry reforming of methane. *Carbon* **2002**, *40*, 1063–1070. [[CrossRef](#)]
42. Branca, C.; Frusteri, F.; Magazzù, V.; Mangione, A. Characterization of carbon nanotubes by TEM and infrared spectroscopy. *J. Phys. Chem. B* **2004**, *108*, 3469–3473. [[CrossRef](#)]



© 2019 by the authors. Licensee MDPI, Basel, Switzerland. This article is an open access article distributed under the terms and conditions of the Creative Commons Attribution (CC BY) license (<http://creativecommons.org/licenses/by/4.0/>).